Biochemistry

 Volume 21, Number 12 June 8, 1982

A Theory of Effects of Protons and Divalent Cations on Phase Equilibria in Charged Bilayer Membranes: Comparison with Experiment†

Bruce R. Copeland‡ and Hans C. Andersen*

ABSTRACT: We summarize the concepts in a recently developed statistical mechanical theory of the effects of proton binding and divalent cation binding on phase equilibria in bilayer membranes composed of acidic phospholipids. The theory is used to calculate membrane phase transition temperatures for different aqueous concentrations of protons, divalent cations, and monovalent salt. We discuss methods for calculating transition temperatures even for systems in which there is not an excess of protons or divalent cations relative to lipids. The results are compared with existing experimental data for a number of lipids. There is good agreement between calculated transition temperature vs. pH curves and experimental data for dimyristoylmethylphosphatidic acid, dimyristoylphosphatidylglycerol, dipalmitoylphosphatidylglycerol, dipalmitoylphosphatidylserine, and dimyristoylphosphatidic acid. General thermodynamic considerations are used to derive a Clapeyron-like equation for the rate of variation in membrane transition temperature with divalent cation concentration. This equation and some available experimental data are used to argue that the large increase in solid to fluid phase transition temperature that is observed experimentally as the divalent cation concentration is increased is the result of a metastable solid phase that exists at low but not high divalent cation concentration. A calculated coexistence diagram is compared with existing experimental data for transition temperatures of dimyristoylphosphatidylglycerol membranes at different total calcium concentrations. Good agreement is obtained when the existence of a metastable solid phase is assumed.

The effects of ions on the phase transition in charged lipid membranes are by now well documented (Tocanne et al., 1974; Verkleij et al., 1974; van Dijck et al., 1975, 1978; Ververgaert et al., 1975; Jacobson & Papahadjopoulos, 1975; Galla & Sackmann, 1975; MacDonald et al., 1976; Träuble & Eibl, 1975; Träuble et al., 1976; Papahadjopoulos et al., 1977; Watts et al., 1978; Newton et al., 1978; Eibl & Blume, 1979), and the relevance of these effects in biological systems has been noted (Verkleij et al., 1974; Jacobson & Papahadjopoulos, 1975; Träuble & Eibl, 1975; MacDonald et al., 1976; Newton et al., 1978). Of particular interest is the dramatic increase in transition temperature that can be induced by concentrations of Ca^{2+} or Mg^{2+} in the millimolar range (Verkleij et al., 1974; van Dijck et al., 1975, 1978; Papahadjopoulos et al., 1977). Significant increases in vesicle fusion and membrane reorganization rates appear to be associated with this increase in transition temperature. These features make the effects of ions on membrane phase transitions especially interesting from a biological point of view.

Several previous workers have presented theories for the effects of protons on phase transitions in charged lipid membranes (MacDonald et al., 1976; Träuble & Eibl, 1975; Träuble et al., 1976; Jähnig, 1976; Forsyth et al., 1977). Recently we developed a statistical mechanical theory for these effects (Copeland, 1979; Copeland & Andersen, 1981a), and the theory was extended to include the effects of divalent cations on such phase transitions (Copeland, 1979; Copeland & Andersen, 1981b).

Here a detailed comparison between the theory and the experimental data of other workers is presented. First we briefly describe the fundamental concepts in our theory. We then compare calculated curves of transition temperature vs. pH with representative experimental data for several different monoprotic and diprotic lipids. Next we use the theory to develop a new interpretation of the effects of divalent cations on membrane phase equilibria. Finally, we compare calculated transition temperatures at different calcium concentrations with experimental data.

Summary of Theory

Monoprotic Lipids. The complete description of the theory and the derivation of equations for monoprotic lipid bilayer membranes were presented previously (Copeland, 1979; Copeland & Andersen, 1981a,b). We begin here with a brief summary of the fundamental concepts in the theory.

For most experiments that are done with bilayer membranes in contact with excess aqueous solution at atmospheric pres-

† From the Department of Chemistry, Stanford University, Stanford, California 94305. *Received January 21, 1981; revised manuscript received December 15, 1981.* This work was supported by grants from the National Institutes of Health (GM 23085) and the National Science Foundation (CHE 78-09317 and CHE 81-07165). B.R.C. was supported in part by a National Science Foundation predoctoral fellowship.

‡ Present address: Division of Medical Genetics, Department of Medicine, School of Medicine, University of Washington, Seattle, WA 98195.

0006-2960/82/0421-2811$01.25/0

sure, the independent thermodynamic variables can be chosen to be the temperature T and the bulk concentrations of the ions in the solution. We designate these bulk ion concentrations by a vector $\mathbf{c}$. The components of $\mathbf{c}$ are the proton concentration c_1, the monovalent cation concentration c_2, the monovalent anion concentration c_3, and the divalent cation concentration c_4. For monoprotic lipid systems in contact with these ions, we assume that each lipid exists in one of the following forms: (1) unbound and bearing a single negative charge; (2) protonated and neutral; (3) bound directly to a divalent cation and bearing a net single positive charge; (4) paired with an adjacent lipid in such a way that the pair is bound (bridged) by a divalent cation. We also assume that bridge binding may require a structural rearrangement of the lipid that makes this type of binding cooperative or anticooperative.

The theory gives laws of mass action for ion binding to lipids in the form

$$K_p(T) = \frac{1 - X_{HL} - X_{CL} - X_{BL}}{X_{HL}} c_1 \exp\left[-\frac{e\psi_0}{kT} - \frac{3e^2\kappa}{2(1 + \kappa b)\epsilon kT} \right] \quad (1a)$$

$$K_C^{-1}(T) = \frac{1 - X_{HL} - X_{CL} - X_{BL}}{X_{CL}} c_4 \exp\left[-\frac{2e\psi_0}{kT} - \frac{2e^2\kappa}{(1 + \kappa b)\epsilon kT} \right] \quad (1b)$$

$$[K_B(a,T)]^{-1} = \frac{(1 - X_{HL} - X_{CL} - X_{BL})^2}{X_{BL}} c_4 \exp[v(a,T)X_{BL}] \exp\left[-\frac{2e\psi_0}{KT} - \frac{4e^2\kappa}{(1 + \kappa b)\epsilon kT} \right] \quad (1c)$$

Here, e is the magnitude of charge on an electron, k is Boltzmann's constant, ϵ is the dielectric constant for water, b is an average ionic diameter, X_{HL}, X_{CL}, and X_{BL} are respectively the mole fractions of protonated lipid, lipid bound directly to divalent cation, and lipid bridged by divalent cation, K_p, K_C, and K_B are respectively the intrinsic proton dissociation constant, the intrinsic divalent cation binding constant, and the intrinsic constant for bridging by divalent cations, and $v(a,T)$ is a measure of the cooperativity of bridge binding (where a is the area per lipid molecule). The factors involving the Gouy–Chapman membrane surface potential ψ_0 and the reciprocal Debye screening length κ enter the equations because of our assumptions about the electrostatic interactions among the ions and lipids. The terms proportional to $\kappa/(\epsilon kT)$ do not appear in laws of mass action used previously by other workers (Träuble & Eibl, 1975; Träuble et al., 1976; Jähnig, 1976; MacDonald et al., 1976). These terms represent the increased Coulombic shielding stabilization of charged membrane species and solution ion species at higher ionic strengths. In these terms in eq 1, we have used extended Debye–Hückel approximations instead of the Debye–Hückel limiting law approximations that were used in our previous work. For high ionic strengths, these extended Debye–Hückel approximations are more accurate than the limiting law approximations.

The laws of mass action (eq 1) are the conditions for chemical equilibrium. At mechanical equilibrium there is an additional condition that the lateral (two-dimensional) pressure must be zero. (For most experiments, the three-dimensional pressure is 1 atm. The corresponding lateral pressure is extremely small and effectively zero.) The lateral pressure can be written as the sum of an "electrostatic pressure" and a "nonelectrostatic pressure". The latter is derived from a nonelectrostatic membrane free energy, which we approximate by a Taylor series expansion (in area and temperature) around the free energy for a fully protonated membrane phase evaluated at its phase transition. The formula for this nonelectrostatic free energy is constructed by using the area, temperature, entropy, lateral compressibility, and thermal expansivity of a fully protonated membrane phase at its phase transition. The laws of mass action, the mechanical equilibrium condition, and the Grahame (1947) equation for the Gouy–Chapman surface potential can be solved for the equilibrium values of the mole fractions, the area, the Gouy–Chapman surface potential, etc. for any membrane phase.

The lipid chemical potential can be derived from the theory in the form

$$\mu_L(\mathbf{c},T) = \mu_{HL}^0(T) + kT \ln (X_{HL}\gamma_a\gamma_e\gamma_c) \quad (2)$$

where μ_{HL}^0 is the chemical potential of protonated lipid in a fully protonated membrane at temperature T. The activity coefficient γ_a reflects nonideality that arises when the area is different from the area for a fully protonated membrane at temperature T; γ_e is an electrostatic activity coefficient; γ_c is a cooperative bridging activity coefficient. Detailed expressions for μ_{HL}^0, γ_a, γ_e, and γ_c were given in our earlier work (Copeland, 1979; Copeland & Andersen, 1981a,b). We note that, under appropriate conditions, the lipid chemical potential μ_L can be interpreted as the chemical potential of protonated lipid (Copeland, 1979; Copeland & Andersen, 1981a).

Each membrane phase is described by a set of the equations that we have discussed. (Of course, each phase is characterized by different values of the thermodynamic properties.) By setting the chemical potentials of two different phases equal, we obtain an expression for the temperature T_t at which these phases coexist in contact with an ionic solution at bulk ion concentration $\mathbf{c}$. This expression for T_t is given in detail in our earlier work. Here we quote an approximate version of the equation that will be useful for discussion purposes.

$$T_t = T_0\Delta S_0/\{\Delta S_0 - k \ln (X_{HL}^f/X_{HL}^s) + (1/2)kX_{BL}^s[(1/2)X_{BL}^s v(a^s,T) + 1]\} \quad (3)$$

In eq 3, the superscripts f and s represent fluid and solid phases, respectively. T_0 and ΔS_0 are the transition temperature and transition entropy per lipid molecule for a fully protonated membrane phase. In writing this approximation, we have taken advantage of the fact that γ_a is approximately 1 and that γ_e is approximately the same for fluid and solid phases. We assume that cooperative bridging by divalent cations does not occur in fluid phases. Equation 3 is an approximate equation that is used only for discussion. Whenever we refer to a transition temperature equation used for calculation of transition temperatures, we are actually referring to the full transition temperature equation derived in our earlier work.

The transition temperature equation is an implicit equation for T_t. An iterative solution beginning with T_t replaced by T_0 on the right side of the equation converges rapidly to an accurate estimate for T_t.

Diprotic Lipids. The theory that we have described was originally developed for monoprotic lipids. In the absence of divalent cations (or divalent cation binding), the equations can be easily extended to apply to diprotic lipids if the two proton binding sites on each lipid are equivalent or if one particular site on the lipid always binds the first proton. The relevant laws of mass action are then

$$K_p''(T) = \frac{1 - X_{H1L} - X_{H2L}}{X_{H1L}} c_1 \exp\left[-\frac{e\psi_0}{kT} - \frac{7e^2\kappa}{2(1 + \kappa b)\epsilon kT} \right] \quad (4a)$$

$$K_p'(T)K_p''(T) = \frac{1 - X_{H1L} - X_{H2L}}{X_{H2L}} c_1^2 \exp\left[-\frac{2e\psi_0}{kT} - \frac{3e^2\kappa}{2(1+\kappa b)\epsilon kT}\right] \quad (4b)$$

where $K_p'(T)$ and $K_p''(T)$ are the first and second proton dissociation constants for the lipid and X_{H1L} and X_{H2L} are the mole fractions of singly and doubly protonated lipid. The corresponding changes in other equations in the theory are straightforward.

Depletion of Ions from Solution. The equations in the theory are most easily applied to experiments in which there is a large excess of solution compared to lipid. Under these conditions, the bulk ion concentrations are not appreciably changed by binding of ions to lipids or association of ions with lipids in the double layer. In practice it is frequently very difficult to make experimental measurements under conditions of a large excess of solution because the nominal lipid concentration becomes very small. In any experiment involving a closed system, it is the number of added ions of each type in the volume rather than the bulk concentrations that is controlled by the experimenter. When the numbers of some ions are comparable to the number of lipids, then changes in the numbers of ions bound to lipids can cause significant changes in the bulk concentrations of these ions. In such situations we therefore say that ions are depleted from solution by binding.

For a given **c**, there is only a single temperature at which a solid phase and a fluid phase can coexist [i.e., at which $\mu_L^f(\mathbf{c},T) = \mu_L^s(\mathbf{c},T)$]. In situations where there is a large excess of solution (no depletion), **c** is effectively constant for fixed *numbers* of ions. Hence the phase transition occurs sharply at a single temperature. Let us next consider a situation where depletion of ions from solution is significant. In general, the mole fractions X_{HL}, X_{CL}, and X_{BL} are different in the solid phase and the fluid phase for fixed values of **c** and T. For fixed values of the *numbers* of ions, the concentration **c** therefore varies whenever the relative amounts of solid and fluid phase vary. As a result, there is not a unique temperature at which solid and fluid coexist for fixed *numbers* of ions when there is depletion. Rather, there is a range of temperatures over which solid and fluid coexist. Of course, the transition temperature equation remains a valid equation for the temperature at which solid and fluid phases are in equilibrium for any given **c**.

There is a simple way to use the transition temperature equation for calculating phase transitions without knowing the relative amounts of the phases, provided that there is an excess of monovalent salt relative to lipid and provided that the nominal lipid concentration is known. Suppose the solid phase is in equilibrium with only an infinitesimal amount of the fluid phase. Then it is possible to relate **c** to the total numbers of ions in the volume (total concentrations) by knowing only the lipid concentration and the values of the mole fractions in the solid phase. In this case the transition temperature equation gives the solidus curve as a function of total concentration of each ion. On the other hand, if the fluid phase is in equilibrium with an infinitesimal amount of solid phase, then it is possible to relate **c** to the total concentrations of ions by knowing only the lipid concentration and the values of the mole fractions in the fluid phase. In this case the transition temperature equation gives the fluidus curve as a function of the total ion concentrations. Thus the transition temperature equation can be used to map out an entire coexistence diagram for transition temperature vs. total ion concentrations. It is this sort of diagram that is usually most closely related to experimental measurements of transition temperature.

Comparison of Theory and Experiment

(A) Proton Binding. (1) Specification of Parameters. In order to use the theory to calculate transition temperature as a function of pH for different lipids, it was necessary to specify the values of a number of parameters. The transition temperature at full protonation, T_0, was obtained from the low pH asymptotic limit of experimental transition temperature vs. pH curves for each lipid. The transition entropy at full protonation, ΔS_0, was taken from experimental transition enthalpy data according to

$$\Delta S_0 = \Delta H_0 / T_0$$

where ΔH_0 is the transition enthalpy per lipid for a fully protonated membrane. In some cases, only transition enthalpies at full deprotonation were available from experiments. The theory can be used to calculate the dependence of the transition enthalpy on the extent of deprotonation, and in most cases that dependence is small (Copeland, 1979). Hence transition enthalpies at full deprotonation were used whenever transition enthalpies at full protonation were unavailable. The intrinsic proton dissociation constant K_p has not been measured for any charged lipids. One of the motivations for developing the theory was to learn how to extract values of this intrinsic constant from measurements of the transition temperature as a function of pH. Thus K_p was adjusted to provide the best fit to experimental transition temperature vs. pH curves. Whenever possible, the curves were fitted by using dissociation constants that were the same for both the fluid phase and the solid phase. The temperature dependence in these constants was ignored since the temperature range in the calculations was generally less than 20 deg. Similarly the dielectric constant ϵ was evaluated at T_0 and treated as a constant. The average ionic diameter b was taken to be 3 Å.

For DMMPA,[1] DMPG, DPPG, DPPS, and DMPA, which are the lipids of interest here, there are no experimental data for bilayer areas at full protonation. The following approach was used to estimate the fluid and solid phase areas at full protonation (a_0^f and a_0^s). We expect that a_0^s should be approximately independent of lipid hydrocarbon chain length for a given lipid head group. However, lipids with different head groups are likely to have different values for a_0^s. The solid phase area for phosphatidylcholine, which is a net neutral lipid, can be estimated from the bilayer thickness data of Janiak et al. (1976) combined with the lipid density data of Nagle & Wilkinson (1978). Just below the phase transition, we estimate the solid-phase area to be 50 Å^2—independent of chain length as expected. Since the head group of phosphatidylserine is comparable in size to phosphatidylcholine, a_0^s was taken to be 50 Å^2 for phosphatidylserine. Phosphatidic acid, methylphosphatidic acid, and phosphatidylglycerol all have head groups that are considerably smaller in size than the phosphatidylcholine head group. Hence a_0^s was arbitrarily chosen to be 44 Å^2 for these lipids. The fluid phase area at full protonation a_0^f can be expected to depend on both the lipid head group type and the lipid hydrocarbon chain length. For this reason, a_0^f was treated as an adjustable parameter in the transition temperature calculations for each lipid.

[1] Abbreviations: DMMPA, dimyristoylmethylphosphatidic acid; DLPG, dilaurylphosphatidylglycerol; DMPG, dimyristoylphosphatidylglycerol; DPPG, dipalmitoylphosphatidylglycerol; DMPS, dimyristoylphosphatidylserine; DPPS, dipalmitoylphosphatidylserine; DMPA, dimyristoylphosphatidic acid; DMPC, dimyristoylphosphatidylcholine; DPPC, dipalmitoylphosphatidylcholine.

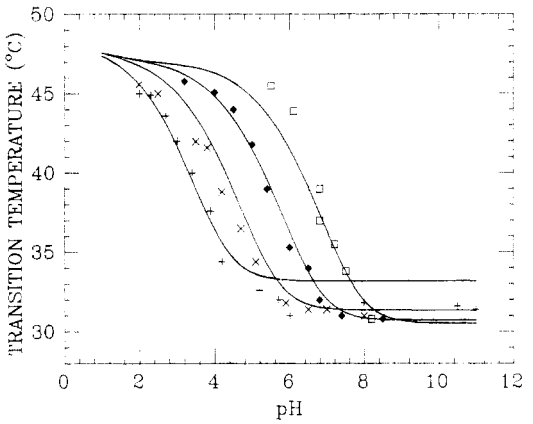

FIGURE 1: Comparison between calculated transition temperature vs. pH curves and experimental data points for DMMPA (Träuble et al., 1976). Monovalent salt concentrations are (+) 2×10^{-1}, (×) 2×10^{-2}, (♦) 2×10^{-3}, and (□) 2×10^{-4} M. Curves were calculated with $a_0^s = 44.0$ Å^2, $a_0^f = 55.5$ Å^2, $a_0^s d_0^s = 210$ dyn/cm, $a_0^f d_0^f = 103$ dyn/cm, $T_0 = 48$ °C, $\Delta S_0 = 17.5$ cal/(mol K), $\epsilon = 70.6$, $b = 3$ Å, and $K_p = 1.25 \times 10^{-2}$ M for both the solid and fluid phase.

Lateral isothermal compressibility data and thermal expansivity data are not available for bilayer membranes. Instead monolayer data was used to estimate these quantities. Values of the lateral compressibility $(a_0 d_0)^{-1}$ were obtained for each phase from phosphatidylcholine and phosphatidylethanolamine pressure vs. area curves (Hui et al., 1975; Phillips & Chapman, 1968; Vilallonga, 1968). The lateral compressibility is independent of area for the solid phase. On the other hand, the lateral compressibility varies somewhat with area in the fluid phase according to the empirical equation

$$a_0^f d_0^f = 325 \text{ dyn/cm} - (4 \times 10^{16} \text{ dyn/cm}^3) a_0^f$$

The lateral compressibility was therefore determined from this equation for the particular value of the area a_0^f used in each calculation. The values of $a_0^s d_0^s$ and $a_0^f d_0^f$ that were used in the calculations are given in the figure legends of Figures 1–4. The monolayer data for thermal expansivity are not very extensive. However, it appears that the thermal expansivity is fairly insignificant, and we therefore neglected these expansivities for all lipids.

(2) Method of Calculation. Transition temperature calculations were performed in the following manner. Values of all parameters were specified, including guesses for a_0^f and K_p^f and K_p^s (the proton dissociation constants in the fluid and solid phases) for each lipid. At each set of ion concentrations c, phase transition temperatures were calculated by iteration of the solid and fluid phase surface potentials and the temperature. These calculated transition temperatures were compared directly with experimental data (in cases where there was no significant depletion of ions). If necessary, the calculations were repeated with different values of a_0^f, K_p^f, and K_p^s in order to obtain the best agreement with experiment for each lipid.

A modification of this procedure was used in cases where there was significant depletion of ions under the experimental conditions. Coexistence temperatures were calculated at different bulk ion concentrations as described above. The lipid concentration and the calculated mole fractions in the solid and fluid phases were then used to compute the total ion concentrations along the solidus and fluidus temperature curves. The resulting coexistence diagrams were compared with experimental data, and the calculations were repeated with different values of a_0^f, K_p^f, and K_p^s in order to get the best agreement with experiment.

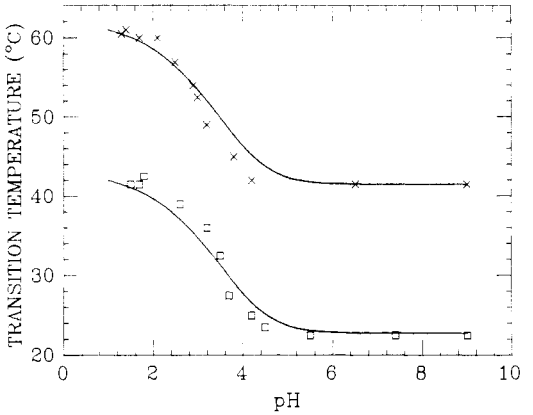

FIGURE 2: Comparison between calculated solidus temperature as a function of pH (—) and the experimental data of van Dijck et al. (1978) for DMPG (□) and DPPG (×). The curve for DMPG was calculated with $a_0^s = 44.0$ Å^2, $a_0^f = 65.0$ Å^2, $a_0^s d_0^s = 210$ dyn/cm, $a_0^f d_0^f = 65$ dyn/cm, $T_0 = 43$ °C, $\Delta S_0 = 21.8$ cal/(mol K), $\epsilon = 72.3$, and $K_p = 2.0 \times 10^{-2}$ M for both the solid and the fluid phase. The curve for DPPG was calculated in the same way but with the following changes in parameters: $a_0^f = 69.0$ Å^2, $a_0^f d_0^f = 49$ dyn/cm, $T_0 = 62$ °C, $\Delta S_0 = 26.9$ cal/(mol K), and $\epsilon = 65.8$. The monovalent salt concentration is 1×10^{-1} M for both curves.

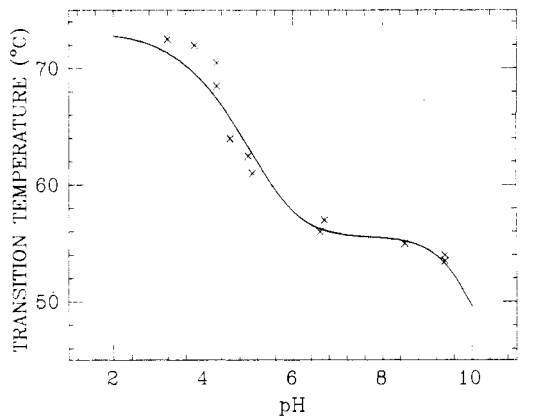

FIGURE 3: Comparison between transition temperatures calculated as a function of pH (—) and experimental data (×) for DPPS (MacDonald et al., 1976). The monovalent salt concentration is 1 $\times 10^{-1}$ M. Calculations were performed with $a_0^s = 50.0$ Å^2, $a_0^f = 70.0$ Å^2, $a_0^s d_0^s = 210$ dyn/cm, $a_0^f d_0^f = 45$ dyn/cm, $T_0 = 73$ °C, $\Delta S_0 = 26.1$ cal/(mol K), $\epsilon = 62.8$, and dissociation constants of $K_p' = 5.0 \times 10^{-4}$ M and $K_p'' = 1 \times 10^{-9}$ M for both the solid and fluid phase.

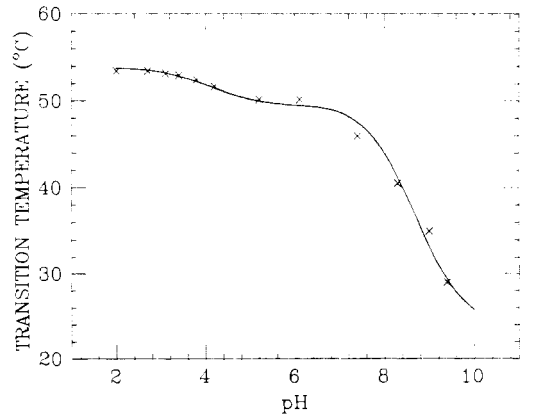

FIGURE 4: Comparison between calculated solidus temperature as a function of pH (—) and experimental data (×) for DMPA (van Dijck et al., 1978). The curve was calculated for $a_0^s = 44.0$ Å^2, $a_0^f = 63.0$ Å^2, $a_0^s d_0^s = 210$ dyn/cm, $a_0^f d_0^f = 73$ dyn/cm, $T_0 = 52$ °C, $\Delta S_0 = 19.9$ cal/(mol K), $\epsilon = 68.8$, and dissociation constants of $K_p'^s = 1.0 \times 10^{-2}$ M, $K_f'^f = 5.5 \times 10^{-3}$ M, and $K_p'' = 1.0 \times 10^{-7}$ M for both the solid and fluid phase.

(3) *Comparison of Calculation and Experiment.* In Figures 1–4, calculated phase transition temperatures are compared with experimental data for a number of different lipids. Figure 1 exhibits transition temperatures at different pH for the monoprotic lipid DMMPA. Experimental data points (Träuble et al., 1976) are shown for four different bulk monovalent salt concentrations. The solid curves in Figure 1 represent transition temperatures that have been calculated from eq 3 with a fluid phase area at full protonation of a_0^f = 55.5 Å^2 and a proton dissociation constant of $K_p = 1.25 \times 10^{-2}$ M that is the same in both phases. In the experimental data, depletion of ions from solution is not a significant problem. In general, there is good agreement between the theory and experiment for monovalent salt concentrations of 2×10^{-3} M or greater. For 2×10^{-4} M monovalent salt concentration, the agreement is not as good. This may be the result of a rather large hysteresis that was found in the experimental data at this low monovalent salt concentration. It may also reflect some difficulties in calculating transition temperature when there is not an excess of salt compared to lipid.

The variation in transition temperature with proton concentration and monovalent salt concentration that is demonstrated in Figure 1 can be understood qualitatively from eq 3, noting that the last term in the denominator is zero in the absence of divalent cations. At low pH the mole fraction of protonated lipid X_{HL} is 1 in both phases. Thus, the transition from solid to fluid occurs at T_0. The principal contribution to the decrease in transition temperature as the pH is raised at constant monovalent salt concentration results from changes in the mole fractions of protonated lipid in each phase. These latter effects can be understood from the law of mass action (eq 1a). When both phases are partially deprotonated, the equilibrium surface charge density is higher in the solid phase because the solid phase has a lower area than the fluid phase. As a result, the potential ψ_0 has a larger magnitide in the solid phase than in the fluid phase. The law of mass action therefore indicates that X_{HL} must be larger in the solid phase than in the fluid phase. We see from eq 3 that this leads to a lowering of the transition temperature relative to T_0. As the pH is increased further, the charge density increases in both phases, and the difference in potential between phases becomes greater. This causes the transition temperature to decrease more. Eventually at high enough pH, both phases are fully deprotonated, and the potential in each phase becomes constant. From eq 1a it follows that the ratio X_{HL}^f/X_{HL}^s remains constant. Thus the transition temperature levels off at high pH. Monovalent salt stabilizes charged species—both in solution and in the membrane—by screening charge. Higher monovalent salt concentrations therefore favor greater degrees of deprotonation in both the solid and fluid membrane phases. This means that at higher monovalent salt concentrations the inflections in transition vs. pH curves are shifted to lower pH, as indicated in Figure 1, and the total shift in transition temperature in going from low pH to high pH is reduced slightly. This latter feature is demonstrated in both the experimental data and calculated results in Figure 1. At high monovalent salt concentrations the calculations appear to overestimate the effect of monovalent salt concentration on the total transition temperature shift. This is presumably due to deficiencies in the Poisson–Boltzmann approximations at high ionic strength.

The overall good agreement between experimental and calculated transition temperatures in Figure 1 is particularly encouraging since only two parameters were adjusted to fit all the data for transition temperature changes. In effect, the value of the fluid phase area a_0^f determines the magnitude of the total transition temperature shift. The value of K_p determines the locations of the inflections in the transition temperature vs. pH curves along the pH axis for all monovalent salt concentrations. The basic shape of the curves and the spacing between curves for different monovalent salt concentrations are intrinsic in the theory.

In Figure 2, calculated transition temperature vs. pH curves are compared with the experimental data of van Dijck et al. (1978) for DMPG and DPPG at 0.1 M monovalent salt. The experimental data were obtained under conditions where depletion of ions is a significant problem. Moreover the lipid concentration in these experiments is unknown, and so it is impossible to calculate complete coexistence diagrams. However, the experiments were performed in such a way that the data points correspond to solidus curves as a function of pH. Calculated solidus curves are therefore presented in Figure 2. There is good agreement between the calculated and experimental data for both lipids. In the calculations, a value of $K_p = 2.0 \times 10^{-2}$ M was used, which is the same for both the solid and the fluid phases for both lipids. The fact that the same value of K_p works for both the 14 carbon chain and 16 carbon chain phosphatidylglycerols is to be expected.

The variation in transition temperature with pH for these two lipids has the same interpretation that was described in connection with Figure 1. In order to obtain the correct calculated transition temperature shifts between full protonation and full deprotonation for both lipids, it was necessary to use a larger fluid-phase area for DPPG than for DMPG. This variation in fluid-phase area with chain length is completely consistent with the fluid-phase areas that we estimate for DPPC and DMPC [using data from Nagle & Wilkinson (1978) and Janiak et al. (1976)].

Watts et al. (1978) have published freeze–fracture electron microscopy data at different pH for DMPG and DPPG. These data indicate that the solid phase just below the solid to fluid membrane phase transition has a rippled texture if the membrane is fully deprotonated. At full protonation, the solid phase has a smooth texture. This might imply that there are two different solid phases—a rippled solid phase and a smooth solid phase. If there are two different solid phases, we should expect to see a discontinuity in the slope of the solid to fluid coexistence line. However, such a discontinuity is not apparent in the experimental data of Figure 2, nor is it discernible in similar experimental data obtained by Watts et al. This suggests that either the transition from the rippled to the smooth solid phase is not a simple, discontinous phase transition or else the rippled and smooth phases have very small differences in thermodynamic properties such as area and enthalpy. In any event, it is possible to explain the experimental data for the variation in solid to fluid phase transition temperature as a function of pH without specifically considering smooth and rippled solid phases.

Figure 3 shows a calculated transition temperature vs. pH curve, which is compared with experimental data for DPPS at 0.1 M monovalent salt (MacDonald et al., 1976). The calculations were performed by using dissociation constants that are identical in both phases. DPPS is a diprotic lipid. First and second proton dissociation constants of $K_p' = 5.0 \times 10^{-4}$ M and $K_p'' = 1.0 \times 10^{-9}$ M were used. In Figure 3, the second deprotonation is only beginning to take place at pH 10, but this is to be expected on the basis of electrostatic considerations.

In addition to the experimental data presented in Figure 3, MacDonald et al. have obtained transition temperature vs. pH data for DPPS in 1.0 M monovalent salt solution and in

distilled water. These data have not been used here because the Poisson–Boltzmann approximations in the theory break down at high ionic strengths, and the theory is difficult to apply to situations where the number of lipids is comparable to the total number of positive monovalent ions.

Figure 4 shows an example of experimental data that cannot be explained by the theory for typical values of solid and fluid phase areas if identical dissociation constants are used in both phases. The data in Figure 4 (van Dijck et al., 1978) are for DMPA (a diprotic lipid) in 0.1 M monovalent salt solution. If the first and second intrinsic proton dissociation constants were the same in both the solid and the fluid phase, the theory would predict that the shift in transition temperature between full protonation and complete single deprontonation should be roughly equal to the shift in transition temperature between complete single deprotonation and full double deprotonation. Instead, the experimental data in Figure 4 show that there is a considerably smaller shift in transition temperature between full protonation and complete single deprotonation than between complete single deprotonation and complete double deprotonation. A similar effect has been observed for other phosphatidic acids (van Dijck et al., 1978; Eibl & Blume, 1979).

The theoretical curve in Figure 4 was calculated by using reasonable values for the solid- and fluid-phase areas at full protonation and by using a second proton dissociation constant that is identical for both phases. The first proton dissociation constant used in the calculation is greater in the solid phase ($K_p'^s = 1.0 \times 10^{-2}$ M) than in the fluid phase ($K_p'^f = 5.5 \times 10^{-3}$ M). As described for Figure 2, the experimental data and calculated curve in Figure 4 correspond to a solidus curve as a function of bulk pH.

It is difficult to understand physically why the first proton dissociation constant should be different in the solid and fluid phases when the second dissociation constant is apparently the same in both phases. X-ray diffraction data for dihexadecylphosphatidic acid have recently been interpreted as indicating that there is only a small (7%) difference in the solid and fluid phase areas at full deprotonation (Jähnig et al., 1979). Such a small difference between solid- and fluid-phase areas is not typical of most lipids. Nevertheless, if the area difference between solid- and fluid-phase phosphatidic acid membranes is really this small, then the experimentally observed small decrease in transition temperature between full protonation and full single deprotonation might be consistent with a first proton dissociation constant K_p' that is the same in both the solid and the fluid phases. In this event, the large transition temperature decrease between full single deprotonation and full double deprotonation might indicate that the second deprotonation constant K_p'' is larger in the fluid phase than in the solid phase. In any case, however, it seems that more extensive experimental investigation of the proton binding, fluid- and solid-phase areas, and transition temperature behavior for phosphatidic acid would be worthwhile.

(*4*) *Additional Discussion of Results.* The values of the solid- and fluid-phase areas at full protonation used in the calculations for Figures 1–4 are given in the figure legends. The fluid-phase areas at full protonation were chosen to provide the best agreement between theory and experiment. The theory predicts that the area in each phase should increase with increasing amounts of deprotonation. Typically, the calculated solid-phase area increases by about 5 Å^2 in going from full protonation to full single deprotonation, and the calculated fluid-phase area increases by about 10 Å^2.

Table I: Intrinsic Proton Dissociation Constants[a]

lipid	K_p' (mol/L)	K_p'' (mol/L)
DMMPA	1.25×10^{-2}	
DMPG[b]	2.0×10^{-2}	
DPPG[b]	2.0×10^{-2}	
DPPS[c]	5.0×10^{-4}	1.0×10^{-9}
DMPA[b]		
solid	1.0×10^{-2}	1.0×10^{-7}
fluid	5.5×10^{-3}	1.0×10^{-7}

[a] Values are those used in the calculations to fit the experimental data in Figures 1–4. [b] The experimental data in Figures 2 and 4 have been interpreted as points along the solidus lines for each lipid. If the experimental data do not correspond to points along the solidus lines but instead correspond to some other path through the coexistence region, then the values of the proton dissociation constants may be inaccurate. [c] There is a large uncertainty in the value of K_p'' because very few experimental data points exist for DPPS at high pH.

The values of the intrinsic proton dissociation constants that have been used in the calculations for the lipids in Figures 1–4 are collected in Table I. These values are insensitive to small errors that may exist in the areas that were used in the calculations—at least for cases where the dissociation constants are the same in both phases. The values of the first proton dissociation constants in Table I are close to 1×10^{-2} M for all lipids except DPPS, for which the first proton dissociation constant is 5×10^{-4} M. These values can be compared with the first dissociation constants for phosphoric and phosphorous acids in solution, which are also close to 1×10^{-2} M. The small value of the first proton dissociation constant for phosphatidylserine may result from interaction between the phosphate group, the carboxyl group, and the amino group of phosphatidylserine. The second proton dissociation constants given in Table I are all about 5 orders of magnitude smaller than the first proton dissociation constants. These ratios are in good agreement with the analogous ratios for other multiprotic acids in solution such as phosphoric acid, phosphorous acid, and sulfurous acid.

(*B*) *Divalent Cation Binding.* (*1*) *Summary of Experimental Data.* Before beginning a detailed comparison of theory and experiment for the variation in transition temperature with divalent cation concentration, it is useful to review the available experimental data. Nearly all experiments have been performed around pH 7, where acidic phospholipids are singly deprotonated. The following qualitative features have been observed for several different acidic phospholipids (Verkleij et al., 1974; van Dijck et al., 1975, 1978; Jacobson & Papahadjopoulos, 1975; MacDonald et al., 1976; Papahadjopoulos et al., 1976, 1977; Newton et al., 1978). At zero divalent cation concentration the transition occurs at a temperature that is about 15–20 deg below T_0 for the particular lipid, as described in the previous section. If the concentration of Mg^{2+} or Ca^{2+} is increased, the transition temperature increases gradually toward T_0. However, when the bulk concentration of these ions reaches the millimolar range, the transition can no longer be observed over a temperature range up to 50 deg above T_0. For phosphatidylserine it has been shown that the membrane is in a solid phase over this temperature range (Newton et al., 1978). This suggests that the transition temperature has been shifted to a temperature much higher than T_0. In fact, for phosphatidylglycerol in the presence of high concentrations of Mg^{2+} or Ca^{2+}, the transition is actually observed at a temperature 50–60 deg above T_0 (Verkleij et al., 1974; van Dijck et al., 1975; Ververgaert et al., 1975). In general, the bulk ion concentration that is required to induce these large increases in transition tem-

perature is greater for Mg^{2+} than for Ca^{2+}. It should also be noted that in the case of phosphatidylglycerol, the transition enthalpy (and entropy) is much greater when the transition temperature is 50–60 deg above T_0 than when the transition temperature is equal to or less than T_0 (van Dijck et al., 1975, 1978; Ververgaert et al., 1975).

Significant morphological changes in membrane structure appear to be associated with the dramatic upward shift in transition temperature at higher Ca^{2+} or Mg^{2+} concentrations (Tocanne et al., 1974; Verkleij et al., 1974; Ververgaert et al., 1975; van Dijck et al., 1975; Jacobson & Papahadjopoulos, 1975; MacDonald et al., 1976; Papahadjopoulos et al., 1976, 1977; Newton et al., 1978). These morphological changes are often described as precipitation. Unfortunately, a clear distinction is seldom made between aggregation of vesicles and structural reorganization of the membranes. In freeze–fracture investigations of phosphatidylglycerol (Ververgaert et al., 1975), the nature of the fluid phase did not seem to change appreciably with divalent cation concentration. However, there was a change in solid-phase morphology between low and high divalent cation concentrations. This suggests that the large increase in transition temperature probably results from some change in solid-phase properties with increasing divalent cation concentration.

As a final matter, it should be noted that for DMMPA, no dramatic upward shift in transition temperature has been observed at higher divalent cation concentrations (Träuble & Eibl, 1975).

(2) Rate of Variation in Transition Temperature with Ion Concentration. We now derive an expression for the rate of variation in transition temperature with divalent cation concentration. The lipid chemical potential μ_L is a function of $\mathbf{c}$ and T. Its total differential is

$$d\mu_L = \left(\frac{\partial \mu_L}{\partial c_1}\right)_{c_2,c_4,T} dc_1 + \left(\frac{\partial \mu_L}{\partial c_2}\right)_{c_1,c_4,T} dc_2 + \left(\frac{\partial \mu_L}{\partial c_4}\right)_{c_1,c_2,T} dc_4 - S_L dT \quad (5)$$

In eq 5 there is no derivative with respect to the anion concentration c_3 because the anion concentration is not an independent variable.

At the solid to fluid phase transition, μ_L is the same in the solid and fluid phases. Suppose that the divalent cation concentration c_4 is varied at constant proton and monovalent cation concentrations. Let us follow the phase transition. Since the solid- and fluid-phase lipid chemical potentials must remain equal to each other at the phase transition, it follows that the change in lipid chemical potential $d\mu_L$ must be the same for both phases. Then, since dc_1 and dc_2 are zero, we can use eq 5 to obtain

$$\frac{dT_t}{d \ln c_4} = \frac{[\partial \mu_L{}^f(\mathbf{c},T_t)/\partial \ln c_4]_{c_1,c_2,T} - [\partial \mu_L{}^s(\mathbf{c},T_t)/\partial \ln c_4]_{c_1,c_2,T}}{\Delta S} \quad (6)$$

In obtaining this result we have used the fact that ΔS, which is the transition entropy per lipid molecule, is equal to $S_L{}^f - S_L{}^s$. (Equations 5 and 6 also hold if μ_L and S_L are interpreted as partial molar quantities rather than partial molecular quantities and ΔS is interpreted as the transition entropy per mole of lipid.) Equation 6 is one member of a class of equations that are analogous to the well-known Clapeyron equation for the rate of change of transition temperature with pressure in a first-order phase transition of a pure substance. Equation 6 is not dependent upon any statistical mechanical model. It follows directly from thermodynamics when the transition is assumed to be of first order.

In order to use eq 6, it is necessary to know $(\partial \mu_L/\partial \ln c_4)_{c_1,c_2,T}$ for each phase. An expression for this quantity can be obtained from our statistical mechanical model. The complete result is given elsewhere (Copeland, 1979). Under most conditions that are of interest here, only one term is important:

$$[\partial \mu_L(\mathbf{c},T)/\partial \ln c_4]_{c_1,c_2,T} \approx -kT[(1/2)X_{BL}{}^* + X_{CL}{}^*] \quad (7)$$

Let us now combine eq 6 and 7 with some experimental data in order to estimate the rate of variation in transition temperature with divalent cation concentration. Experimental transition entropies are in the range 20–40 cal/(mol K). Suppose we take 30 cal/(mol K) as a reasonable estimate. A reasonable upper limit for the difference in $(\partial \mu_L/\partial \ln c_4)_{c_1,c_2,T}$ between fluid and solid is provided by assuming that the fraction of bound divalent cation per lipid is 0 for the fluid and 0.5 for the solid. Under these conditions, eq 6 and 7 predict that a 10-fold increase in bulk divalent cation concentration should produce at most a 25–30-deg increase in transition temperature. This prediction is in pronounced disagreement with experiment. For Ca^{2+} and Mg^{2+}, experiment shows that less than a 10-fold increase in divalent cation concentration can produce shifts in transition temperature that are in excess of 50–60 deg (MacDonald et al., 1976; Papahadjopoulos et al., 1976, 1977). Moreover, experimental binding data imply that the actual difference in the fraction of bound divalent cation per lipid between phases is considerably less than the value of 0.5 that was used in the calculation (Papahadjopoulos et al., 1977). This would make the predicted rate of variation in transition temperature even smaller. Inclusion of other terms in $(\partial \mu_L/\partial \ln c_4)_{c_1,c_2,T}$ not shown in eq 7 does not improve the agreement since these terms tend to decrease the predicted rate of change in transition temperature with divalent cation concentration.

Equation 6 can be used in another way. We can combine experimental estimates for the transition entropy and the rate of variation in transition temperature in order to estimate the difference in $(\partial \mu_L/\partial \ln c_4)_{c_1,c_2,T}$ between phases. Using 30 cal/(mol K) for the transition entropy and a rate of change in transition temperature of 60 deg per factor of 10 increase in divalent cation concentration, we estimate that the difference in $(\partial \mu_L/\partial \ln c_4)_{c_1,c_2,T}$ between phases must be greater than 1 kT (around room temperature). This seems like an extremely large change in this quantity between phases for the following reasons. First, consider the variation in chemical potential of a solute in solution with respect to the logarithm of its own concentration. This derivative is approximately kT (as long as there is no extreme variation in activity coefficient with concentration of the solute). In the case under consideration here, we are interested in the *difference* between phases in the variation of lipid chemical potential with respect to the logarithm of the concentration of *another species* (a divalent cation) in solution. It is hard to imagine that the magnitude of this *difference* could be greater than kT unless there is some extreme variation in nonideality with respect to the divalent cation concentration for one of the phases. Moreover, it should be noted that even when there *is* extreme nonideality that depends on divalent cations, the nonideality does not necessarily contribute much to $(\partial \mu_L/\partial \ln c_4)_{c_1,c_2,T}$. For instance, in the model described above (even when there is cooperative divalent cation bridging) the principal contribution to $[\partial \mu_L/\partial \ln c_4)_{c_1,c_2,T}$ is still the ratio of bound divalent cation per lipid times kT. In this model, therefore, cooperative bridging by divalent cations can only contribute to $(\partial \mu_L/\partial \ln c_4)_{c_1,c_2,T}$ by increasing

the ratio of bound divalent cation per lipid, and this ratio can only be increased to a certain limit that is determined by the stoichiometry of calcium binding. It is conceivable that a polyion that could bind many divalent cations might have a large variation in its chemical potential with respect to the logarithm of the divalent cation concentration. However, the lipids that we are considering are not polyions. In fact, electrostatic considerations suggest that on the average only one divalent cation should bind for every *two* lipids. None of these arguments prove that $\Delta(\partial\mu_L/\partial \ln c_4)_{c_1,c_2,T}$ cannot be larger than kT, but they do suggest that such large values are unlikely.

The arguments presented here indicate that the large increase in transition temperature that is observed experimentally is unlikely at thermodynamic equilibrium and hence may correspond to nonequilibrium behavior. In particular, the transition temperature (in the vicinity of T_0) at intermediate divalent cation concentrations may represent a transition from a metastable solid phase to the fluid phase. At higher divalent cation concentrations, the stable solid-phase forms, and the transition from solid to fluid phase occurs at a much higher temperature. We shall use this interpretation in comparing theoretical and experimental transition temperatures at different divalent cation concentrations. It is worth noting that there is some experimental evidence of metastability for divalent cation concentrations that are close to the concentration where there is a large increase in transition temperature (Ververgaert et al., 1975).

(*3*) *Comparison of Calculation and Experiment.* The most extensive experimental data for variation in transition temperature with divalent cation concentration are for phosphatidylglycerol in the presence of varying amounts of Mg^{2+} and Ca^{2+} at pH 7 (Verkleij et al., 1974; van Dijck et al., 1975, 1978; Ververgaert et al., 1975). In these experiments the total divalent cation concentration, rather than the bulk divalent cation concentration, was controlled externally. In addition, the experiments were done under conditions where the bulk monovalent salt concentration is not in excess. This means that the bulk concentration of monovalent salt changes with the bulk (or total) divalent cation concentration because divalent cations displace monovalent counterions from the double layer.

In Figure 5, a calculated coexistence diagram of transition temperature vs. total calcium concentration is compared with experimental data for DMPG (van Dijck et al., 1975). In the calculations, bridging was assumed to occur only in the solid phase, and K_B and v were taken as constants that are independent of temperature and area. The calculations were performed in much the same way as described earlier for proton binding, but in this case the bulk concentration of Ca^{2+} was varied, and the pH was held constant. It was necessary to iterate X_{BL}^s in order to solve eq 1c. Total calcium concentrations were calculated by combining the amount of calcium bound to lipid, the amount of Ca^{2+} in the bulk of solution, and the amount of Ca^{2+} in the double layer. This latter quantity was determined by using an approximation [see Copeland (1979)], but the approximation is not very important since the double layer contribution to the total calcium concentration is considerably less than the contribution from binding of calcium. The concentration of monovalent salt was obtained by summing the concentration of added monovalent salt and the concentration of monovalent salt displaced from the double layer by calcium (bound and in the double layer). All necessary quantities were iterated to self-consistency in the calculations.

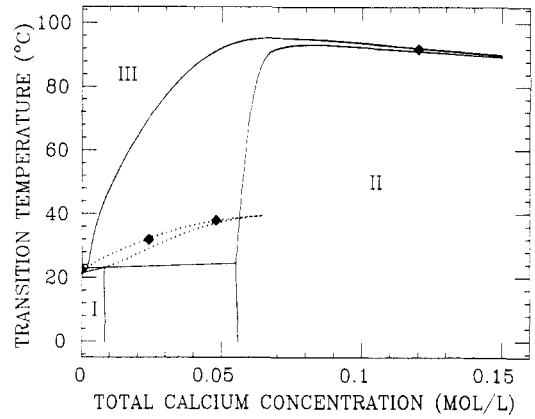

FIGURE 5: Comparison between experimental data of van Dijck et al. (1975) for DMPG (♦) and a coexistence diagram calculated for a model with cooperative bridging in the solid phase. Region I is a solid phase with negligible bridging; region II is a solid phase with extensive bridging; region III is the fluid phase. The unlabeled regions are the conditions under which two of these phases can coexist, the upper region corresponding to coexistence of II and III and the lower region corresponding to coexistence of I and II. The dotted lines represent the metastable continuation of the fluidus and solidus lines for the transition from solid I to fluid III. These lines actually extend out to 0.150 mol/L total calcium concentration, but the extension has not been shown in the diagram. The dotted lines give the transition region that would be observed if for some reason solid phase II did not form. The concentration of added monovalent salt is 0.018 M, and the proton concentration is $c_1 = 1.0 \times 10^{-7}$ M. The lipid concentration is 0.120 mol/L. The calculations were performed with $K_C = 1.0\ M^{-1}$ for both the solid and the fluid phases and with $K_B = 2.9 \times 10^{-2}\ M^{-1}$ and $v = 22$ in the solid phase. The ratio W_L/d_L was taken to be 0.8 M^{-1}. All other parameters were the same as in the calculations for DMPG in Figure 2.

All parameters in the calculations (except for K_C, K_B, and v) were taken from the previous calculations for proton binding to DMPG (see Figure 2). The parameters K_C, K_B, and v were varied to give the best agreement between calculation and experiment. For simplicity, there parameters were chosen to be independent of temperature. We expect that the use of a more reasonable temperature dependence of the equilibrium constants would not change any of the qualitative features on Figure 5.

The large cooperativity constant used in Figure 5 gives rise to a phase transition between two solid phases—a solid phase with negligible calcium bridging, which appears at low calcium concentrations (region I in Figure 5), and a solid phase with extensive bridging ($X_{BL} \sim 0.9$–1.0), which appears at higher calcium concentrations (region II). The regions between I, II, and III (enclosed by solid lines) are two-phase regions that separate the phases I–III. The nearly horizontal line at about 24 °C is a three-phase coexistence line for solid I, solid II, and fluid III. In Figure 5 the bulk monovalent salt concentration is not constant but instead increases from 0.018 M at zero total calcium concentration to about 0.140 M at high calcium concentration. This means that Figure 5 is a coexistence diagram but not a phase diagram. It is therefore technically incorrect to apply tie-line constructions to the two-phase regions in Figure 5. This change in monovalent salt concentration with calcium concentration also explains why the three-phase line in Figure 5 is not strictly horizontal. Nevertheless, calculations in which the bulk concentration of monovalent salt is fixed (not shown here) give true phase diagrams that look very similar to Figure 5. It may therefore be convenient to think of Figure 5 as a phase diagram.

The dotted lines in Figure 5 represent a metastable continuation of the two-phase region for the transition from solid

I to fluid III. This is the transition behavior that would be observed if the stable solid phase II did not form until higher divalent cation concentrations were reached. Indeed, some of the experimental data points fall in this metastable transition region. At higher calcium concentrations the experimental transition temperature coincides with the equilibrium curve in Figure 5.

The calculated phase behavior in Figure 5 can be understood in the following way. At zero bulk (and total) Ca^{2+} concentration, the transition from solid to fluid phase occurs at a temperature that is about 20 deg below T_0, as described under Proton Binding. At low calcium concentrations in the equilibrium part of Figure 5 and at higher calcium concentrations in the metastable part of Figure 5, the transition temperature increases gradually toward T_0 when the calcium concentration is increased. This behavior is quite similar to the variation in transition temperature with proton concentration that was described earlier, and the explanation is similar. At higher calcium concentrations, cooperative binding of calcium causes the appearance of a second solid phase (solid II). At high enough calcium concentrations, cooperative bridging by calcium causes the mole fraction of bridged lipid to be very close to 1.0 in solid II. This greatly decreases the mole fraction of protonated lipid in solid II, stabilizes solid II relative to the fluid, and causes the transition temperature to be much higher than T_0. The gradual decrease in calculated transition temperature above 0.06 M total calcium concentration is caused by increases in the ionic strength. These increases in ionic strength result from increases in the bulk concentrations of calcium and monovalent salt. Such increases in ionic strength slightly destabilize calcium bridging relative to direct binding in solid II. This in turn destablizes solid II relative to the fluid and lowers the transition temperature.

Figure 5 is presented to demonstrate one type of model that can explain the experimental variation in transition temperature with divalent cation concentration. The agreement between theory and experiment in Figure 5 is good provided we assume that some of the experimental data at low calcium concentrations represent metastable behavior. This assumption can also be used to explain other transition temperature data for DMPG in the presence of Mg^{2+} (van Dijck et al., 1975) and for DLPG in the presence of Ca^{2+} (Verkliej et al., 1974). It is important to recognize that the values of K_C, K_B, and v that were used to construct Figure 5 do not provide a unique fit to the experimental data. A variety of reasonably large values for K_C agree with experimental data below 0.06 mol/L total calcium (along the metastable curve in Figure 5), and above 0.06 mol/L total calcium there is a range of different combinations of K_B and v that give essentially the same transition temperature (along the equilibrium curve in Figure 5).

There are two features in the theoretical calculations in Figure 5 that are particularly worth emphasizing. The first is the large stabilization of the solid phase relative to the fluid phase at higher divalent cation concentrations. This stabilization results because differences in the binding of divalent cations in the two phases cause the mole fraction of protonated lipid to be much smaller in the solid phase than in the fluid phase. The second feature that should be emphasized is the manner in which metastability can explain the experimental data. The model in Figure 5 provides a good demonstration of this. The arguments that suggest metastability in the experimental data are based largely on eq 6 combined with some experimental data and reasonable assumptions about the magnitude of variations in the lipid chemical potential with changes in bulk ion concentrations. These arguments are not very model dependent. We can expect that other models for ion binding may also be in agreement with the experimental data if the existence of transition from a metastable solid phase to a stable solid phase is invoked to explain the abrupt rise in transition temperature at higher divalent cation concentrations. In this regard, it should be noted that a significant increase in fusion of phosphatidylserine vesicles has been observed at calcium concentrations near the concentration that is required to induce a large increase in membrane transition temperature (Papahadjopoulos et al., 1976, 1977). This suggests a possible connection between vesicle fusion and a transition from a metastable solid phase to a stable solid phase. Such a transition may play an important role in fusion events.

Acknowledgments

We thank Dr. John C. Owicki for a number of helpful suggestions regarding the calculations.

References

Copeland, B. R. (1979) Ph.D. Thesis, Stanford University, Stanford, CA.

Copeland, B. R., & Andersen, H. C. (1981a) *J. Chem. Phys. 74*, 2536.

Copeland, B. R., & Andersen, H. C. (1981b) *J. Chem. Phys. 74*, 2548.

Eibl, H., & Blume, A. (1979) *Biochim. Biophys. Acta 553*, 476.

Forsyth, P. A., Jr., Marcelja, S., Mitchell, D. J., & Ninham, B. W. (1977) *Biochim. Biophys. Acta 469*, 335.

Galla, H. J., & Sackmann, E. (1975) *J. Am. Chem. Soc. 97*, 4114.

Grahame, D. C. (1947) *Chem. Rev. 41*, 441.

Hui, S. W., Cowden, M., Papahadjopoulos, D., & Parsons, D. F. (1975) *Biochim. Biophys. Acta 382*, 265.

Jacobson, K., & Papahadjopoulos, D. (1975) *Biochemistry 14*, 152.

Jähnig, F. (1976) *Biophys. Chem. 4*, 309.

Jähnig, F., Harlos, K., Vogel, H., & Eibl, H. (1979) *Biochemistry 18*, 1459.

Janiak, M. J., Small, D. M., & Shipley, G. G. (1976) *Biochemistry 15*, 4575.

MacDonald, R. C., Simon, S. A., & Baer, E. (1976) *Biochemistry 15*, 885.

Nagle, J. F., & Wilkinson, D. A. (1978) *Biophys. J. 23*, 159.

Newton, C., Pangborn, W., Nir, S., & Papahadjopoulos, D. (1978) *Biochim. Biophys. Acta 506*, 281.

Papahadjopoulos, D., Vail, W. J., Pangborn, W. A., & Poste, G. (1976) *Biochim. Biophys. Acta 448*, 265.

Papahadjopoulos, D., Vail, W. J., Newton, C., Nir, S., Jacobson, K., & Poste, G. (1977) *Biochim. Biophys. Acta 465*, 579.

Phillips, M. C., & Chapman, D. (1968) *Biochim. Biophys. Acta 163*, 159.

Tocanne, J. F., Ververgaert, P. H. J. Th., Verkleij, A. J., & van Deenen, L. L. M. (1974) *Chem. Phys. Lipids 12*, 201.

Träuble, H., & Eibl, H. (1975) in *Functional Linkage in Biomolecular Systems* (Schmitt, F. O., Schneider, D. M., & Crothers, D. M., Eds.) pp 59–102, Raven Press, New York.

Träuble, H., Teubner, M., Woolley, P., & Eibl, H. (1976) *Biophys. Chem. 4*, 319.

van Dijck, P. W. M., Ververgaert, P. H. J. Th., Verkleij, A. J., van Deenen, L. L. M., & de Gier, J. (1975) *Biochim. Biophys. Acta 406*, 465.

van Dijck, P. W. M., de Kruijff, B., Verkleij, A. J., van Deenen, L. L. M., & de Gier, J. (1978) *Biochim. Biophys. Acta 512*, 84.
Verkleij, A. J., de Kruijff, B., Ververgaert, P. H. J. Th., Tocanne, J. F., & van Deenen, L. L. M. (1974) *Biochim. Biophys. Acta 339*, 432.
Ververgaert, P. H. J. Th., de Kruijff, B., Verkleij, A. J., Tocanne, J. F., & van Deenen, L. L. M. (1975) *Chem. Phys. Lipids 14*, 97.
Vilallonga, F. (1968) *Biochim. Biophys. Acta 163*, 159.
Watts, A., Harlos, K., Maschke, W., & Marsh, D. (1978) *Biochim. Biophys. Acta 510*, 63.

Effect of Cytochrome b_5 on the Transbilayer Distribution of Phospholipids in Model Membranes†

J. R. Nordlund, C. F. Schmidt, P. W. Holloway, and T. E. Thompson*

ABSTRACT: The transbilayer distribution of phosphatidylethanolamine was assessed in phosphatidylcholine–phosphatidylethanolamine vesicles that contained various amounts of cytochrome b_5. The small vesicles, made by sonication, and the large vesicles, made by ethanol injection, were fractionated by centrifugation before cytochrome b_5 was asymmetrically incorporated into the bilayer. The mole ratio of phospholipid to protein ranged from 280 to 560 in the small vesicles and from 100 to 500 in the large vesicles. The phosphatidylethanolamine distribution, determined by chemical labeling with trinitrobenzenesulfonic acid, was assessed in vesicles that contained intact cytochrome b_5 molecules and in vesicles where only the hydrophobic tail remained associated with the bilayer. At every phospholipid to protein ratio examined, the transbilayer distribution of phosphatidylethanolamine in either the small or large unilamellar vesicles was not significantly different from the distribution in control vesicles that contained no protein. Ethanol was added to some cytochrome b_5–vesicle preparations (20% v/v) in an attempt to facilitate rearrangement of the phospholipids. No differences in the transbilayer distribution were observed. These results are discussed in terms of transbilayer equilibrium and the perturbation induced by the protein.

Phospholipids are usually asymmetrically distributed across biological membranes [see review by op den Kamp (1979)], but this biological phenomenon is often not observed in simple phospholipid bilayers (Nordlund et al., 1981a,b). Since proteins are another major component of biological membranes, it is possible that their interactions with the phospholipids influence the transbilayer phospholipid distribution. In a biological system, where proteins are inserted into preexisting bilayers, one plausible model for the generation of lipid asymmetry would have two components. The protein would first have to create a new transbilayer distribution through preferential interactions with specific types of lipids or by changing the packing constraints within the bilayer. Second, since transmembrane phospholipid movement (flip-flop) is slow in model systems, but fast in many biological membranes (op den Kamp, 1979; Rothman & Lenard, 1977), the protein, or other factors already present, would have to facilitate rapid flip-flop in order to allow the new system to rearrange.

In this study, we have simulated the biological condition by asymmetrically incorporating an integral membrane protein into preformed small or large unilamellar vesicles composed of phosphatidylcholine and phosphatidylethanolamine. Cytochrome b_5, an enzyme whose in vivo function is to participate in electron transfer reactions while bound to the endoplasmic reticulum (Holloway & Katz, 1972; Shimakata et al., 1972; Strittmatter et al., 1974), was chosen as a prototypic membrane protein because it possesses several characteristics that make it amenable to phospholipid asymmetry studies: it is an integral membrane protein, it forms monomeric or octameric aqueous solutions in the absence of lipid or detergent (Spatz & Strittmatter, 1971; Calabro et al., 1976), and it spontaneously inserts into phospholipid bilayers (Strittmatter et al., 1972; Sullivan & Holloway, 1973; Leto & Holloway, 1979).

The following structural and functional characteristics of cytochrome b_5 are pertinent to this study. It is an amphipathic protein comprised of a hydrophilic domain (M_r = 11 000) and a hydrophobic moiety (M_r = 5000) joined by a short flexible peptide sequence (Visser et al., 1975; Tajima et al., 1978). Denaturation studies revealed that these domains are structurally independent. The hydrophilic portion, which is stabilized by a noncovalently bound heme, unfolded first, without affecting the structure of the hydrophobic domain. Further denaturation caused the protein octamers to dissociate into monomers, suggesting that the tertiary structure of the hydrophobic domain had been altered (Tajima et al., 1976). The functional responsibilities are also segregated; proteolytic cleavage by trypsin separated the catalytic capabilities, which reside solely in the hydrophilic domain, from the membrane binding hydrophobic fragment. It is worth noting that proteolysis did not induce significant conformational changes in either the membrane-bound fragment or the soluble hydrophilic moiety (Tajima et al., 1978). The orientation of the hydrophobic domain in the bilayer has been a disputed issue, but recent experiments appear to demonstrate that the carboxyl terminus is on the same side of the membrane as the hydrophilic domain (Dailey & Strittmatter, 1981).

† From the Department of Biochemistry, University of Virginia School of Medicine, Charlottesville, Virginia 22908. *Received October 8, 1981.* This investigation was supported by U.S. Public Health Service Grants GM-14628, GM-23573, GM-17452, and GM-23858.

0006-2960/82/0421-2820$01.25/0